

Use of Pretreatment Perfusion MRI–based Intratumoral Heterogeneity to Predict Pathologic Response of Triple-Negative Breast Cancer to Neoadjuvant Chemoimmunotherapy

Toulsie Ramtobul, MD • Victoire Lepagney, MD • Claire Bonneau, MD, PhD • Maxime Jin, MD • Emmanuelle Menet, MD • Juliette Sauge, MD • Enora Laas, MD • Emanuela Romano, MD, PhD • Diana Bello-Roufai, MD • Fatima Mechta-Grigoriou, PhD • Anne Vincent Salomon, MD • François-Clément Bidard, MD, PhD • Adriana Langer, MD • Caroline Malhaire, MD • Luc Cabel, MD, PhD • Hervé J. Brisse, MD* • Anne Tardivon, MD*



From the Department of Radiology (T.R., V.L., M.J., C.M., H.J.B., A.T.), Department of Diagnostic and Theranostic Medicine–Pathology (J.S., A.V.S.), Department of Surgical Oncology (E.L.), Department of Medical Oncology (E.R.), Stress and Cancer Laboratory (F.M.G.), and INSERM U830 (F.M.G.), Institut Curie, PSL University, 26 rue d'Ulm, 75005 Paris, France; Department of Surgical Oncology and INSERM U900, Statistical Methods for Precision Medicine, Institut Curie, University of Versailles Saint-Quentin-en-Yvelines, Saint-Cloud, France (C.B.); Departments of Diagnostic and Theranostic Medicine–Pathology (E.M.), Medical Oncology (D.B.R., F.C.B., L.C.), and Radiology (A.L.), Institut Curie, PSL University, Saint-Cloud, France; Department of Immunology, PSL University, Paris, France (E.R.); and Circulating Tumor Biomarkers Laboratory, Department of Translational Research, Institut Curie, Paris, France (F.C.B.). Received February 26, 2024; revision requested March 25; final revision received June 3; accepted June 14. **Address correspondence** to T.R. (email: toulsie.ramtobul@curie.fr).

Supported by Institut Curie.

* H.J.B. and A.T. are co-senior authors.

Conflicts of interest are listed at the end of this article.

See also the editorial by Rauch in this issue.

Radiology 2024; 312(3):e240575 • <https://doi.org/10.1148/radiol.240575> • Content codes:  

Background: Neoadjuvant chemoimmunotherapy (NACI) has significantly increased the rate of pathologic complete response (pCR) in patients with early-stage triple-negative breast cancer (TNBC), although predictors of response to this regimen have not been identified.

Purpose: To investigate pretreatment perfusion MRI–based radiomics as a predictive marker for pCR in patients with TNBC undergoing NACI.

Materials and Methods: This prospective study enrolled women with early-stage TNBC who underwent NACI at two different centers from August 2021 to July 2023. Pretreatment dynamic contrast-enhanced MRI scans obtained using scanners from multiple vendors were analyzed using the Tofts model to segment tumors and analyze pharmacokinetic parameters. Radiomics features were extracted from the rate constant for contrast agent plasma-to-interstitial transfer (or K^{trans}), volume fraction of extravascular and extracellular space (V_e), and maximum contrast agent uptake rate ($Slope_{max}$) maps and analyzed using unsupervised correlation and least absolute shrinkage and selector operator, or LASSO, to develop a radiomics score. Score effectiveness was assessed using the area under the receiver operating characteristic curve (AUC), and multivariable logistic regression was used to develop a multimodal nomogram for enhanced prediction. The discrimination, calibration, and clinical utility of the nomogram were evaluated in an external test set.

Results: The training set included 112 female participants from center 1 (mean age, 52 years \pm 11 [SD]), and the external test set included 83 female participants from center 2 (mean age, 47 years \pm 11). The radiomics score demonstrated an AUC of 0.80 (95% CI: 0.70, 0.89) for predicting pCR. A nomogram incorporating the radiomics score, grade, and Ki-67 yielded an AUC of 0.86 (95% CI: 0.78, 0.94) in the test set. Associations were found between higher radiomics score (>0.25) and tumor size ($P < .001$), washout enhancement ($P = .01$), androgen receptor expression ($P = .009$), and programmed death ligand 1 expression ($P = .01$), demonstrating a correlation with tumor immune environment in participants with TNBC.

Conclusion: A radiomics score derived from pharmacokinetic parameters at pretreatment dynamic contrast-enhanced MRI exhibited good performance for predicting pCR in participants with TNBC undergoing NACI, and could potentially be used to enhance clinical decision making.

© RSNA, 2024

Supplemental material is available for this article.

Stage I–III triple-negative breast cancer (TNBC) accounts for approximately 15%–20% of new diagnoses of early breast cancer (1). Until 2021, the standard of care according to American and European guidelines for patients with early-stage TNBC with diameter 10 mm or greater and/or nodal involvement was anthracycline- and taxane-containing neoadjuvant chemotherapy (NAC) (2,3). The response to NAC provides prognostic information as pathologic

complete response (pCR) (ie, the absence of invasive cancer in the breast and axillary nodes [ypT0/Tis ypN0]) after NAC is strongly associated with improved long-term disease-free survival and overall survival in patients with TNBC (4).

The KEYNOTE-522 phase III trial demonstrated that the addition of pembrolizumab, an anti-programmed death 1 monoclonal antibody, to standard NAC regimens

This copy is for personal use only. To order copies, contact reprints@rsna.org

Abbreviations

AUC = area under the receiver operating characteristic curve, NAC = neoadjuvant chemotherapy, NACI = neoadjuvant chemoimmunotherapy, pCR = pathologic complete response, TNBC = triple-negative breast cancer

Summary

A radiomics score derived from pretreatment perfusion MRI effectively predicted pathologic complete response in participants with early-stage triple-negative breast cancer following neoadjuvant chemoimmunotherapy.

Key Results

- In a prospective dual-center study involving 195 women with early-stage triple-negative breast cancer (TNBC), a radiomics score derived from pharmacokinetic maps predicted pathologic complete response after neoadjuvant chemoimmunotherapy (area under the receiver operating characteristic curve [AUC] in the test set, 0.80).
- A nomogram incorporating the radiomics score, grade, and Ki-67 demonstrated improved predictive performance, with an AUC of 0.86 in the test set.
- The radiomics score was associated with programmed death ligand 1 expression ($P = .01$), demonstrating a correlation with tumor immune environment in participants with TNBC.

clearly improved pCR at the time of surgery (64.8% in the neoadjuvant chemoimmunotherapy [NACI] group vs 51.2% in the NAC group; $P < .001$) (5) and event-free survival at 36 months (84.5% in the NACI group vs 76.8% in the NAC group; $P < .001$) (6). However, this improvement came with an increase in toxicity (5,6). Identifying reliable predictors of the response to immunotherapy in this setting is therefore warranted, and further efforts are needed to clarify the effective roles of programmed death ligand 1 combined positive score,

tumor mutational burden, and tumor-infiltrating lymphocyte count (7–9).

In TNBC, intratumoral heterogeneity commonly manifests at the histologic and genetic levels (10,11). Spatial heterogeneity plays a crucial role in driving cancer progression and promoting resistance to systemic therapies (12). Dynamic contrast-enhanced MRI techniques with semiquantitative or quantitative parameters offer valuable data within tumor regions that directly reflect biologic information related to proliferation activity, cellularity, or microvasculature (13). Recent studies have shown that intratumoral heterogeneity assessed using clustering or voxel-wise radiomics approaches on native images or kinetic maps is a significant predictor of response and recurrence-free survival in patients with breast cancers treated with NAC (14,15). However, its potential role in assessing response to immunotherapy-based regimens for TNBC has not been explored.

This study was designed to assess whether perfusion MRI–based intratumoral heterogeneity, measured with radiomics at pretreatment dynamic contrast-enhanced MRI, is associated with pCR after NACI in patients with TNBC.

Materials and Methods

This dual-center prospective study was approved by the Institut Curie ethics review board (study DATA20277), and written informed consent was obtained from all participants prior to enrollment. This study complied with the tenets of the Declaration of Helsinki and the Standards for Reporting of Diagnostic Accuracy Studies, or STARD, criteria (16).

Study Sample

Consecutive patients (aged ≥ 18 years) with biopsy-proven early-stage TNBC—at clinical stage T2 or higher (diameter ≥ 20 mm)

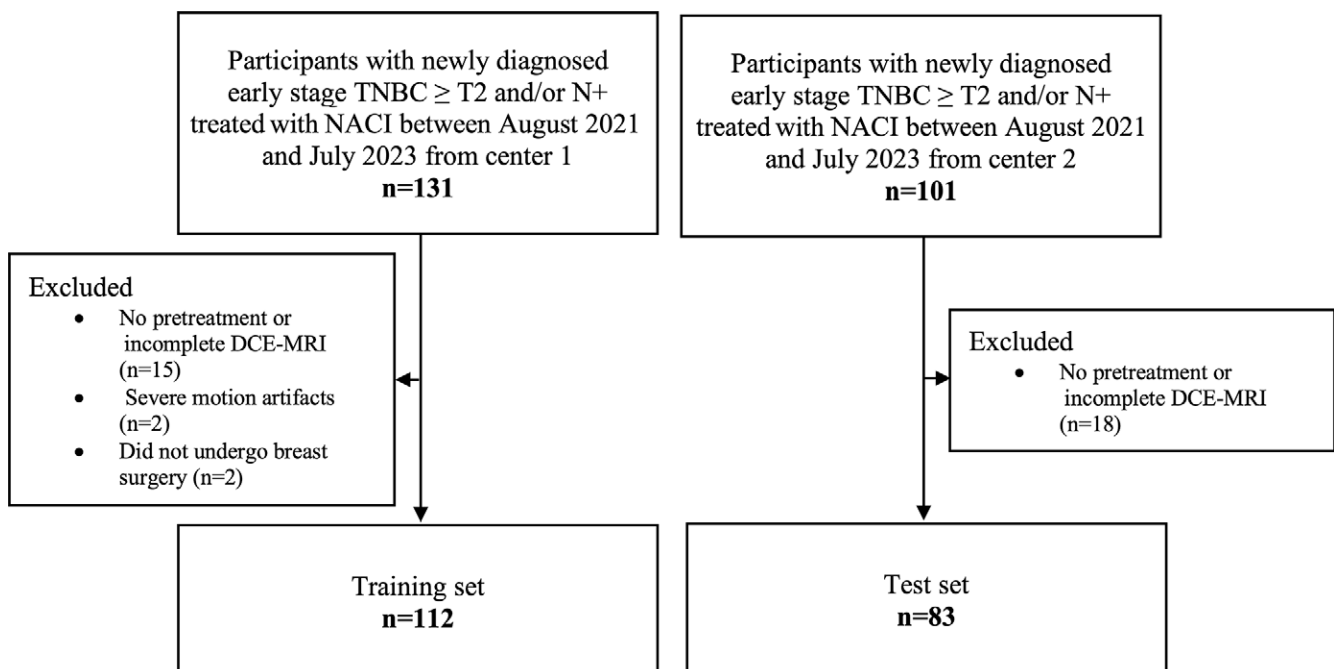


Figure 1: Flowchart of the inclusion and exclusion criteria. DCE = dynamic contrast enhanced, N+ = node positive, NACI = neoadjuvant chemoimmunotherapy, TNBC = triple-negative breast cancer.

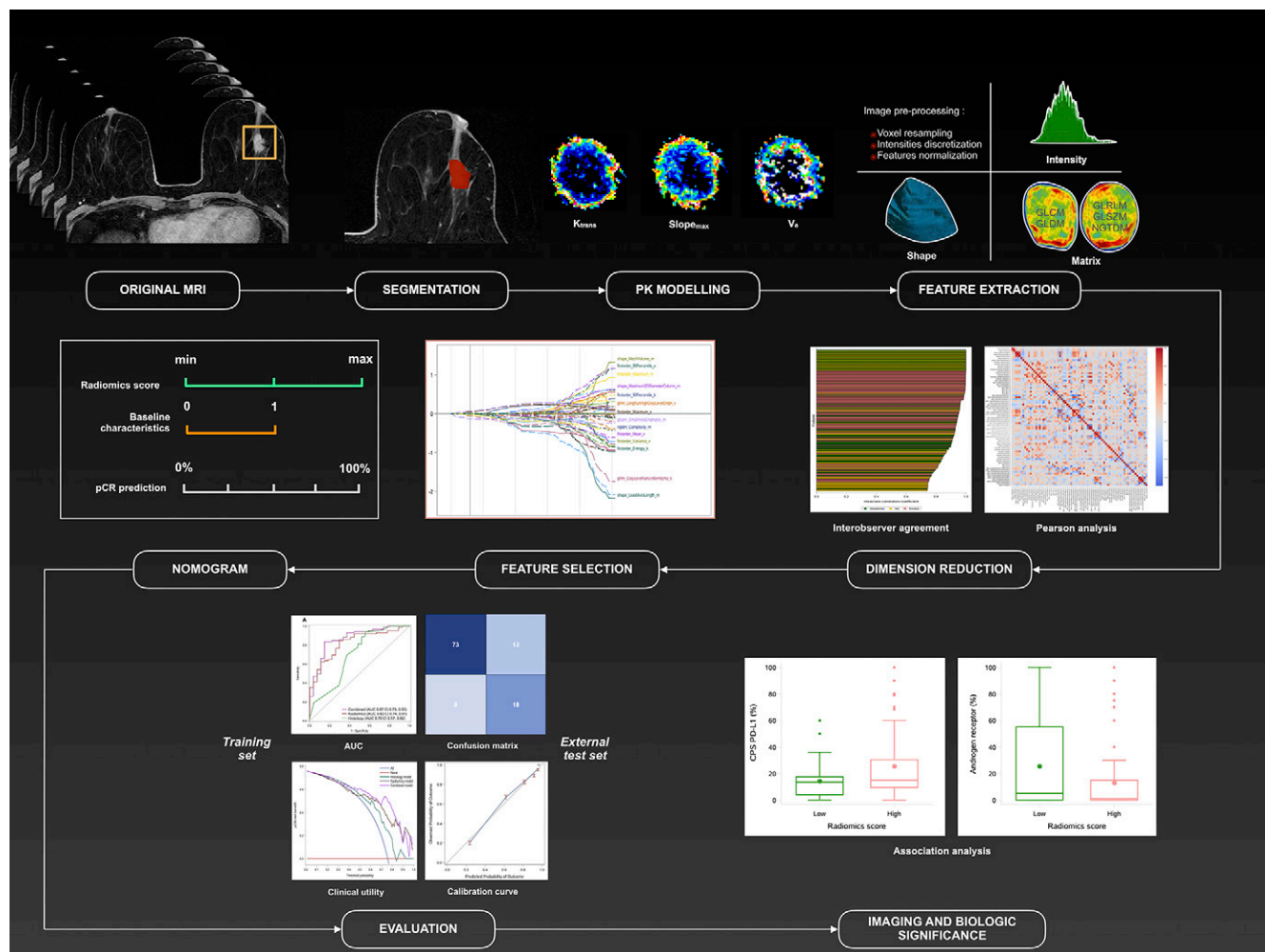


Figure 2: Diagram of the radiomics pipeline used for the prediction of pathologic complete response (pCR) at perfusion MRI. Three pharmacokinetic (PK) maps were built based on Tofts modeling. Radiomics features were extracted from each pharmacokinetic map. After Pearson correlation analysis, interobserver agreement analysis, and least absolute shrinkage and selector operator, or LASSO, selection, the most relevant features were included in a logistic regression to construct a radiomics score. A nomogram comprising the radiomics score and baseline characteristics was established for the prediction of pCR in the training set. The performance of the model was evaluated in both the training and external test sets. Exploratory analyses were also conducted to determine the interpretability of the radiomics score. AUC = area under the receiver operating characteristic curve, CPS = combined positive score, GLCM = gray level co-occurrence matrix, GLDM = gray level dependence matrix, GLRLM = gray level run length matrix, GLSZM = gray level size zone matrix, NGTDM = neighboring gray tone difference matrix, PD-L1 = programmed death ligand 1.

and/or node positive—who started treatment with NACI between August 2021 and July 2023 at two tertiary care centers were prospectively included. The exclusion criteria were as follows: absence of pretreatment dynamic contrast-enhanced MRI, inadequate MRI scan acquisition, or no breast surgery (Fig 1). The initial planned NACI treatment comprised four cycles of pembrolizumab every 3 weeks plus paclitaxel plus carboplatin, followed by four cycles of pembrolizumab plus doxorubicin or epirubicin plus cyclophosphamide.

MRI Procedure and Image Evaluation

Pretreatment breast MRI scans were obtained using various scanner models and field strengths at the two centers. The pulse sequences, contrast injection procedure, and timing of data acquisition were in line with those used in the I-SPY 2 trial. Sequence parameters are listed in Table S1 (17).

Two radiologists (T.R. and V.L., with 6 and 1 year of experience in breast MRI, respectively) evaluated the MRI scans

according to the Breast Imaging Reporting and Data System (18) lexicon. Semiautomatic tumor volume segmentation using the 3D Slicer (version 4.10) Grow From Seeds algorithm was performed by a board-certified radiologist (T.R.) based on the first dynamic contrast-enhanced T1-weighted images. Coil artifacts were manually excluded during this process. For multifocal lesions, only the largest mass was considered for image analysis and segmentation. The dynamic contrast-enhanced MRI time-course data from the tumor mask were fitted with a one-compartment two-parameter standard Tofts model (19). The 3D Slicer PkModeling module (20) was used to generate voxel-based parametric maps for K_{trans} (rate constant for contrast agent plasma-to-interstitial transfer), V_e (volume fraction of extravascular and extracellular space), and $Slope_{max}$ (maximum contrast agent uptake rate) using a measured arterial input function selecting the internal thoracic artery (Appendix S1). Interobserver reproducibility was assessed by having another board-certified radiologist (M.J., with 4 years of breast

Table 1: Baseline Characteristics of the Study Sample

Characteristic	Training Set (n = 112)	Test Set (n = 83)	P Value
Mean age (y)*	52 ± 11	47 ± 11	.02
Age			.21
≤50 y	56 (50)	49 (59)	
>50 y	56 (50)	34 (41)	
Menopausal status			.09
Premenopausal	55 (49)	51 (61)	
Postmenopausal	57 (51)	32 (39)	
Clinical tumor stage			.47
T1 or T2	86 (77)	60 (72)	
T3 or T4	26 (23)	23 (28)	
Clinical nodal stage			.12
Node negative	69 (62)	42 (51)	
Node positive	43 (38)	41 (49)	
Grade			.10
II	10 (9)	14 (17)	
III	102 (91)	69 (83)	
Mean Ki-67 (%)*	63 ± 22	64 ± 23	.76
Ki-67			.92
≤75%	68 (61)	51 (61)	
>75%	44 (39)	32 (39)	
Mean TILs (%)*	26 ± 24	27 ± 25	.65
TILs			.50
≤20%	65 (58)	47 (57)	
>20%	46 (41)	27 (32)	
NA	1 (1)	9 (11)	
NACI without treatment interruption or dose reduction			.25
Yes	96 (86)	66 (80)	
No	16 (14)	17 (20)	
Breast surgery			.02
Lumpectomy	82 (73)	47 (57)	
Mastectomy	30 (27)	36 (43)	
Axillary surgery			<.001
Sentinel lymph node	76 (68)	35 (42)	
Axillary dissection	36 (32)	48 (58)	
pCR			.13
Yes	84 (75)	54 (65)	
No	28 (25)	29 (35)	

Note.—Categorical data are presented as numbers of women, with percentages in parentheses. *P* values were calculated using the χ^2 test or Fisher exact test for categorical variables. NA = not available, NACI = neoadjuvant chemoimmunotherapy, pCR = pathologic complete response, TIL = tumor-infiltrating lymphocyte.

* Continuous data are presented as means ± SDs. *P* values were calculated using the Wilcoxon-Mann-Whitney or Student *t* test.

Table 2: Imaging Findings of the Study Sample

Finding	Training Set (n = 112)	Test Set (n = 83)	P Value
Breast density			.34
A or B	49 (44)	42 (51)	
C or D	63 (56)	41 (49)	
Glandular enhancement			.09
High	11 (10)	15 (18)	
Low	101 (90)	68 (82)	
Tumor site			.41
Right breast	54 (48)	45 (54)	
Left breast	58 (52)	38 (46)	
Number of lesions			.58
Single	81 (72)	57 (69)	
Multiple	31 (28)	26 (31)	
Mean largest tumor size (mm)*†	33 ± 13	33 ± 16	.54
Largest tumor size*			.39
≤20 mm	14 (13)	14 (17)	
>20 mm	98 (88)	69 (83)	
Intratumoral T2 hypersignal			.17
Absent	34 (30)	33 (40)	
Present	78 (70)	50 (60)	
Internal enhancement			.15
Homogeneous	9 (8)	12 (14)	
Heterogeneous	103 (92)	71 (86)	
Enhancement curve			.004
Ascendant or plateau	64 (57)	64 (77)	
Washout	48 (43)	19 (23)	
Associated nonmass enhancement			.08
Absent	60 (54)	55 (66)	
Present	52 (46)	28 (34)	
Peritumoral T2 hypersignal			.48
Absent	21 (19)	19 (23)	
Present	91 (81)	64 (77)	
Malignant calcifications			.50
Absent	83 (74)	65 (78)	
Present	29 (26)	18 (22)	

Note.—Categorical data are presented as numbers of women, with percentages in parentheses. *P* values were calculated using the χ^2 test or Fisher exact test for categorical variables.

* Largest tumor size was determined on initial standard postcontrast dynamic contrast-enhanced MRI scans.

† Mean largest tumor size is a continuous variable, presented as mean ± SD. *P* value was calculated using the Wilcoxon-Mann-Whitney test.

MRI experience) independently perform tumor segmentation on 45 randomly chosen lesions from the training set.

Radiomics Feature Extraction

A total of 107 Image Biomarker Standardization Initiative–compliant features (Table S2) were extracted from each

parametric map using Python PyRadiomics (version 3.0.1) (21). Before feature extraction, outliers (more than 3 SDs from the mean value) were removed, voxel size was resampled to 0.7 × 0.7 × 0.7 mm using trilinear interpolation, and gray-level discretization with fixed bin width size was performed using PyRadiomics. No feature harmonization method was

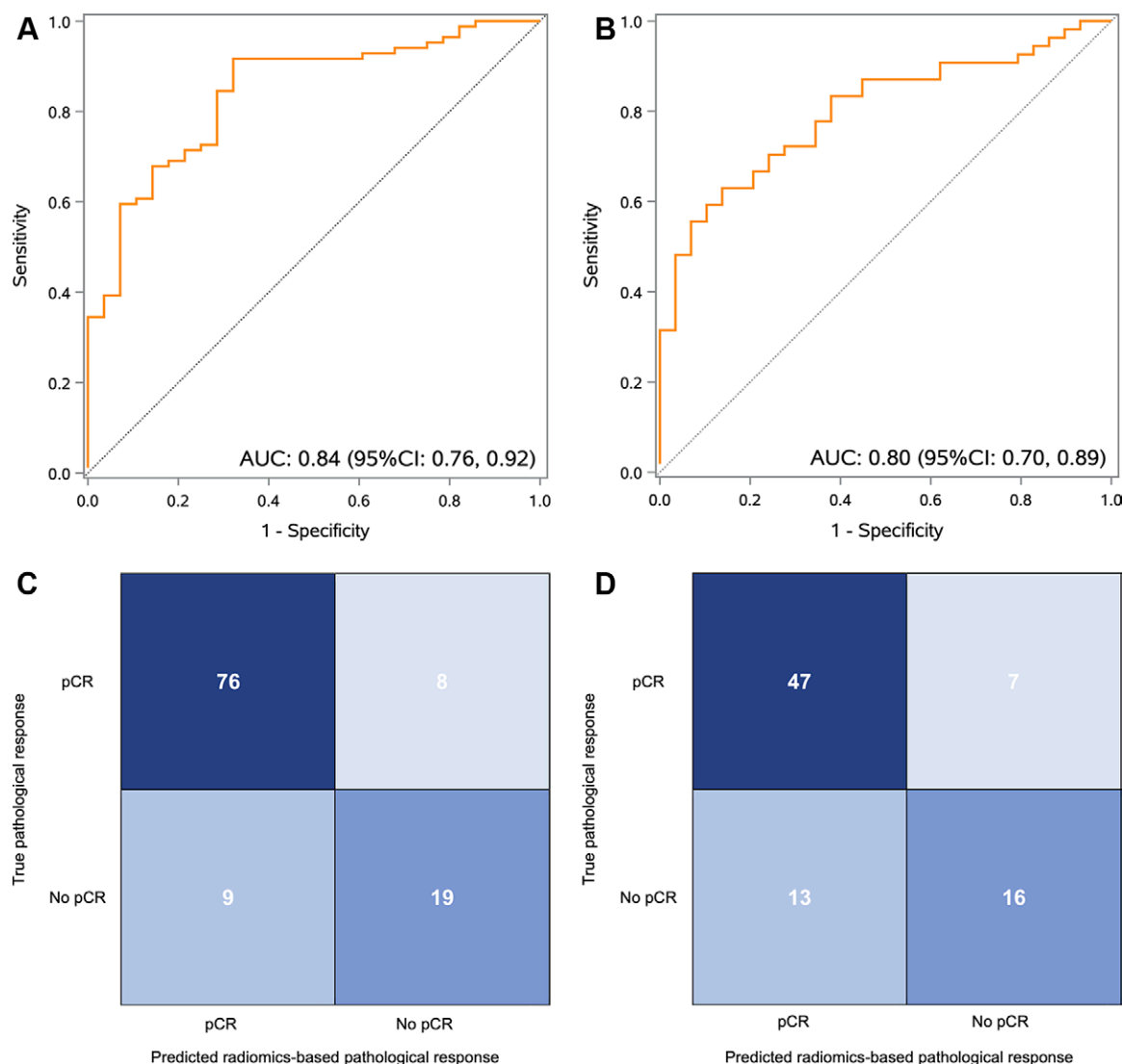


Figure 3: (A, B) Receiver operating characteristic curves of the radiomics score for predicting pathologic complete response (pCR) in the (A) training set and (B) external test set. (C, D) Confusion matrices of the optimal cutoff value, 0.25, of the radiomics score determined in (C) the training set and assessed in (D) the external test set. AUC = area under the receiver operating characteristic curve.

used to correct for the batch effect introduced by machine models.

Feature Selection and Predictive Model Construction

Only radiomics features with a two-way random absolute agreement intraclass correlation coefficient, or ICC(2,1), value of 0.75 or greater were included in subsequent analyses. The strength of agreement for intraclass correlation coefficient values was interpreted as follows: below 0.50, poor; 0.50–0.74, moderate; 0.75–0.89, good; and 0.90 or above, excellent. Clusters of features with a Pearson correlation coefficient greater than 0.90 were collapsed into one representative feature to reduce multicollinearity. Variable selection employed 10-fold cross-validation with the least absolute shrinkage and selection operator, or LASSO, method. A radiomics score was derived from the linear combination of selected features weighted by their respective coefficients. All of the code used for radiomics modeling and data analysis has

been deposited into a publicly accessible repository (https://www.github.com/Toulsie/mri_radiomics_TNBC) (Fig 2).

Statistical Analysis

Continuous variables were analyzed using Wilcoxon-Mann-Whitney and Student *t* tests according to the normality of the distribution. Categorical variables were analyzed using the χ^2 test or Fisher exact test. The area under the receiver operating characteristic curve (AUC) was calculated for the radiomics score, and optimal cutoffs for identifying pCR were derived using the Youden index. Bootstrapped CIs are reported. Given the null hypothesis of an AUC of 0.50, the alternate hypothesis of an AUC of 0.75, a pCR proportion of 65%–70%, and a statistical power of 90%, the minimum required sample size in the external test set was 80 participants. The calibration of the different models was assessed using calibration curves plotted from bootstrapping with 1000 resamples, accompanied by the Hosmer-Lemeshow

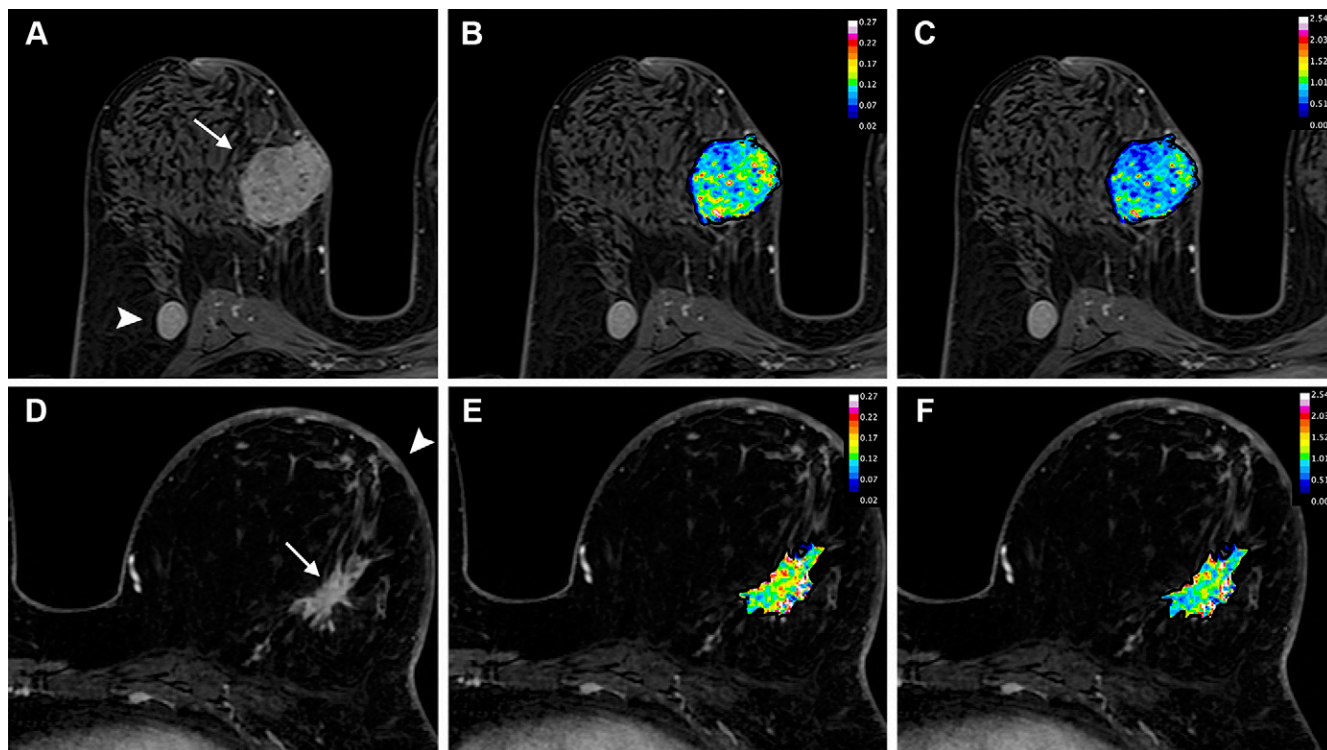


Figure 4: Axial dynamic contrast-enhanced MRI scans obtained in two women before they underwent neoadjuvant chemioimmunotherapy (NACI) for triple-negative breast cancer. **(A)** T1-enhanced MRI scan, **(B)** rate constant for contrast agent plasma-to-interstitial transfer (K^{trans}) map, and **(C)** maximum contrast agent uptake rate ($Slope_{max}$) map in a 56-year-old woman whose tumor manifested as a spherical 4-cm mass enhancement (arrow in **A**) in the right breast with axillary node involvement (arrowhead in **A**). The radiomics score was high, at 3.3. Histopathologic examination after NACI revealed no invasive residual cancer in the breast or the lymph nodes (pathologic complete response). **(D)** T1-enhanced MRI scan, **(E)** K^{trans} map, and **(F)** $Slope_{max}$ map in a 49-year-old woman whose tumor manifested as a spiculated 3-cm mass enhancement (arrow in **D**) in the left breast with thickening of the skin (arrowhead in **D**). The parametric maps show much greater spatial heterogeneity than in the case shown in **B** and **C**, with areas of high intensity. The radiomics score was low, at -1.6 . Histopathologic examination after NACI revealed a 10-mm invasive residual cancer in the breast (not pathologic complete response).

goodness-of-fit test. Decision curve analysis was used to calculate the net benefit of the use of the radiomics model at different threshold probabilities in both sets. Radiomics and statistical analyses were performed by one author (T.R., with 8 years of experience performing statistical analysis) using Python (version 3.7.4; Python Software Foundation) and SAS (version 9.4; SAS Institute) software. All statistical tests were two sided, and $P < .05$ was considered indicative of statistical significance.

Results

Study Participant Characteristics

A total of 195 female participants were included: 112 (mean age, 52 years \pm 11 [SD]) from center 1 (training set) and 83 (mean age, 47 years \pm 11) from center 2 (external test set), as outlined in Figure 1. The distribution of surgical interventions (mastectomy vs lumpectomy) revealed a higher prevalence of mastectomy in the external test set than in the training set (43% [36 of 83] vs 27% [30 of 112]; $P = .02$). Similarly, axillary lymph node dissection (as opposed to sentinel lymph node biopsy) was more common in the external test set than in the training set (58% [48 of 83] vs 32% [36 of 112]; $P < .001$) (Table 1). MRI analysis indicated a lower rate of washout enhancement curve in the external test set than in the test set (23% [19 of 83] vs 43% [48 of 112]; $P =$

.004) (Table 2). Overall, 83% (162 of 195) of the participants completed NACI without treatment interruption or dose reduction. The pCR rate was 71% (138 of 195): 75% (84 of 112) and 65% (54 of 83) in the training and test sets, respectively ($P = .13$).

Predictive Model Development and Testing

In the reproducibility analysis of the K^{trans} , V_e , and $Slope_{max}$ maps within the training set, 85, 52, and 54 radiomics features, respectively, demonstrated an intraclass correlation coefficient of 0.75 or greater (Fig S1). Among the features not correlated with each other (Fig S2), the least absolute shrinkage and selection operator logistic regression model was subsequently used to select features with nonzero coefficients to derive a radiomics score (Table S3). This radiomics score achieved an AUC of 0.84 (95% CI: 0.76, 0.92) for predicting pCR in the training set (Fig 3). With an optimal cutoff of 0.25, sensitivity (recall) was 0.91 (95% CI: 0.84, 0.97) (76 of 84 participants), specificity was 0.68 (95% CI: 0.51, 0.85) (19 of 28 participants), positive predictive value (precision) was 0.89 (95% CI: 0.83, 0.96) (76 of 85 participants), negative predictive value was 0.70 (95% CI: 0.53, 0.88) (19 of 27 participants), and F1 score was 0.90 (Table S4).

In the test set, the radiomics score achieved an AUC of 0.80 (95% CI: 0.70, 0.89) for predicting pCR. The same optimal cutoff of 0.25 had a sensitivity (recall) of 0.87 (95% CI: 0.78, 0.96)

Table 3: Univariable and Multivariable Analysis of the Training Data Set to Assess Pathologic Complete Response

Variable	Univariable Analysis		Multivariable Analysis	
	Odds Ratio	P Value	Odds Ratio	P Value
Age	1.0 (0.9, 1.0)	.41		
Menopausal status (postmenopausal vs premenopausal)	0.9 (0.4, 2.0)	.74		
Clinical tumor stage (T3 or T4 vs T1 or T2)	0.5 (0.2, 1.4)	.20		
Clinical nodal stage (node positive vs node negative)	0.6 (0.3, 1.5)	.31		
Grade (III vs II)	9.0 (2.1, 37.8)	.003	8.2 (1.2, 56.0)	.03
Ki-67	1.0 (1.0, 1.1)	.004	1.0 (1.0, 1.1)	.03
TILs	1.0 (1.0, 1.0)	.54		
Breast density (C or D vs A or B)	1.4 (0.6, 3.3)	.44		
Glandular enhancement (high vs low)	0.5 (0.1, 2.0)	.36		
Number of lesions (multiple vs single)	0.6 (0.2, 1.5)	.27		
Largest tumor size	1.0 (1.0, 1.0)	.75		
Intratumoral T2 hypersignal (present vs absent)	1.1 (0.4, 2.8)	.81		
Internal enhancement (heterogeneous vs homogeneous)	0.8 (0.2, 4.3)	.84		
Enhancement curve (washout vs ascendant or plateau)	2.9 (1.1, 7.4)	.03		
Associated nonmass enhancement (present vs absent)	0.5 (0.2, 1.1)	.08		
Peritumoral T2 hypersignal (present vs absent)	0.4 (0.1, 1.6)	.22		
Malignant calcifications (present vs absent)	0.5 (0.2, 1.3)	.17		
Radiomics score	2.7 (1.8, 4.2)	<.001	2.8 (1.7, 4.4)	<.001
NACI without treatment interruption or dose reduction (yes vs no)	2.8 (0.9, 8.3)	.07		

Note.—Data in parentheses are 95% CIs. Only variables identified as significant ($P < .05$) in the univariable analysis were included in the multivariable analysis, after backward selection. NACI = neoadjuvant chemoimmunotherapy, TIL = tumor-infiltrating lymphocyte.

(47 of 54 participants), specificity of 0.55 (95% CI: 0.37, 0.73) (16 of 29 participants), positive predictive value (precision) of 0.78 (95% CI: 0.68, 0.89) (47 of 60 participants), negative predictive value of 0.70 (95% CI: 0.51, 0.88) (16 of 23 participants), and F1 score of 0.83. Two example cases illustrating the added value of the radiomics score are shown in Figure 4.

Integrating Radiomics and Clinical Data

In the training set, only tumor grade III versus II ($P = .003$), Ki-67 ($P = .004$), washout enhancement curve ($P = .03$), and radiomics score ($P < .001$) were associated with pCR in the univariable analysis and were therefore included in the multivariable analysis (Table 3). Tumor grade (odds ratio, 8.2 [95% CI: 1.2, 56.0]; $P = .03$), Ki-67 (odds ratio, 1.0 [95% CI: 1.0, 1.1]; $P = .03$), and radiomics score (odds ratio, 2.8 [95% CI: 1.7, 4.4]; $P < .001$) maintained their association with pCR in the multivariable analysis.

A nomogram model was developed that incorporated the two independent histologic predictors (tumor grade and Ki-67) along with the radiomics score (Fig S3). All receiver operating characteristic curves are provided in Figure 5. In the training set, the nomogram model had an AUC of 0.89 (95% CI: 0.81, 0.96), which was greater than that of the histologic prediction model (incorporating tumor grade and Ki-67) (AUC, 0.68 [95% CI: 0.55, 0.81]; $P < .001$). In the test set, the nomogram model yielded an AUC of 0.86 (95% CI: 0.78, 0.94), again outperforming the histologic prediction model (AUC, 0.77 [95% CI: 0.67, 0.88]; $P = .03$). The calibration curves of the nomogram model demonstrated good concordance between predicted and observed pCR in both sets. The Hosmer-Lemeshow

test showed no departure from a good fit, with a P value of .30 and .97 in the training and external test sets, respectively.

Clinical Use

The decision curve analysis results for the radiomics, histologic, and nomogram models aimed at predicting pCR are presented in Figure 6. These findings demonstrate that both the radiomics and nomogram models surpass the treat-all and treat-none schemes, as well as the model based solely on histologic data. Specifically, the radiomics and nomogram models offer a more substantial benefit in predicting pCR when considering a wide range of threshold probabilities above 50%.

Exploring the Imaging and Biologic Significance of the Radiomics Score

Cancers with a higher radiomics score (>0.25) were associated with a smaller tumor size (28 mm vs 38 mm; $P < .001$) (Fig S4) and a higher rate of washout enhancement curve (39% [57 of 145] vs 20% [10 of 50]; $P = .01$) compared with those with a lower radiomics score. Androgen receptor expression and combined positive score for programmed death ligand 1 were available for 140 (72%) and 119 (61%) of the 195 participants, respectively (Table S5). Among these participants, tumors with a higher radiomics score (>0.25) were more likely to have lower expression of androgen receptor ($\leq 75\%$) (95% [98 of 103] vs 81% [30 of 37]; $P = .009$) and higher programmed death ligand 1 combined positive score ($>20\%$) (40% [36 of 91] vs 14% [four of 28]; $P = .01$) than tumors with a lower radiomics score (Table S6). There was a positive association between pCR and both higher programmed death ligand 1 combined positive score (odds ratio, 4.9 [95% CI: 1.6,

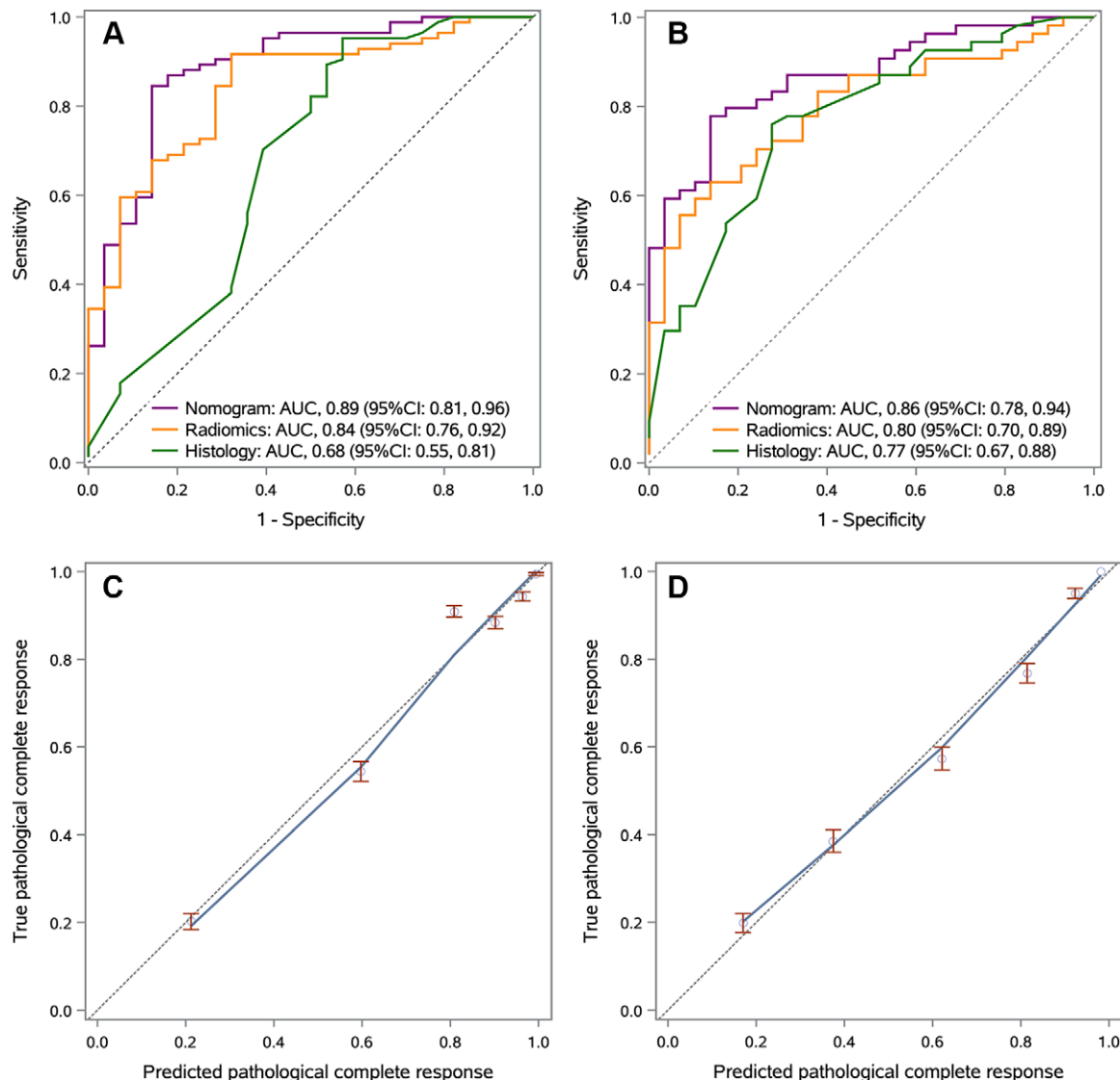


Figure 5: (A, B) Receiver operating characteristic curves for the radiomics score alone, the histologic predictors (tumor grade and Ki-67) alone, and the nomogram incorporating the radiomics score and the histologic predictors for predicting pathologic complete response in the (A) training set and (B) external test set. (C, D) Calibration curves of the nomogram in the (C) training set and (D) external test set. Calibration curves were plotted using bootstrapping with 1000 resamples. AUC = area under the receiver operating characteristic curve.

15.3]; $P = .006$) and lower expression of androgen receptor (odds ratio, 4.2 [95% CI: 1.2, 14.2]; $P = .02$).

Discussion

This study examined imaging predictors of treatment response within the context of neoadjuvant chemoimmunotherapy (NACI) in triple-negative breast cancer (TNBC). While the incorporation of immune checkpoint inhibitors has notably increased the rate of pathologic complete response (pCR) in patients with early-stage disease, the indication for immunotherapy in TNBC relies on a uniform approach, neglecting the potential benefits of tailoring treatment based on individual tumor characteristics. The proposed radiomics score, derived from images obtained using various “real-life” MRI scanner models, demonstrated favorable discrimination and clinical utility for predicting pCR in both the training set (area under the receiver operating characteristic curve [AUC], 0.84) and

the test set (AUC, 0.80). The nomogram model combining the radiomics score with the pretreatment histologic variables tumor grade and Ki-67 (a proliferation index) showed further improvement in performance and outperformed the prediction model with histologic predictors alone (AUC, 0.86 vs 0.77 in the test set; $P = .03$). Tumors with high rates of proliferation are often more susceptible to cytotoxic therapies, such as chemotherapy. Furthermore, chemotherapeutic agents have been found to exhibit immunomodulatory properties, which can lead to a more inflamed tumor microenvironment, potentially enhancing the likelihood of achieving pCR with immunotherapy in a synergistic manner (22). The high positive predictive value of the optimal radiomics score cutoff suggests the potential of the score as an imaging marker for future de-escalation studies. Notably, up to 75% of patients with TNBC receiving NACI experience grade 3 or higher adverse events (5). Omitting anthracyclines from a NACI regimen displayed a

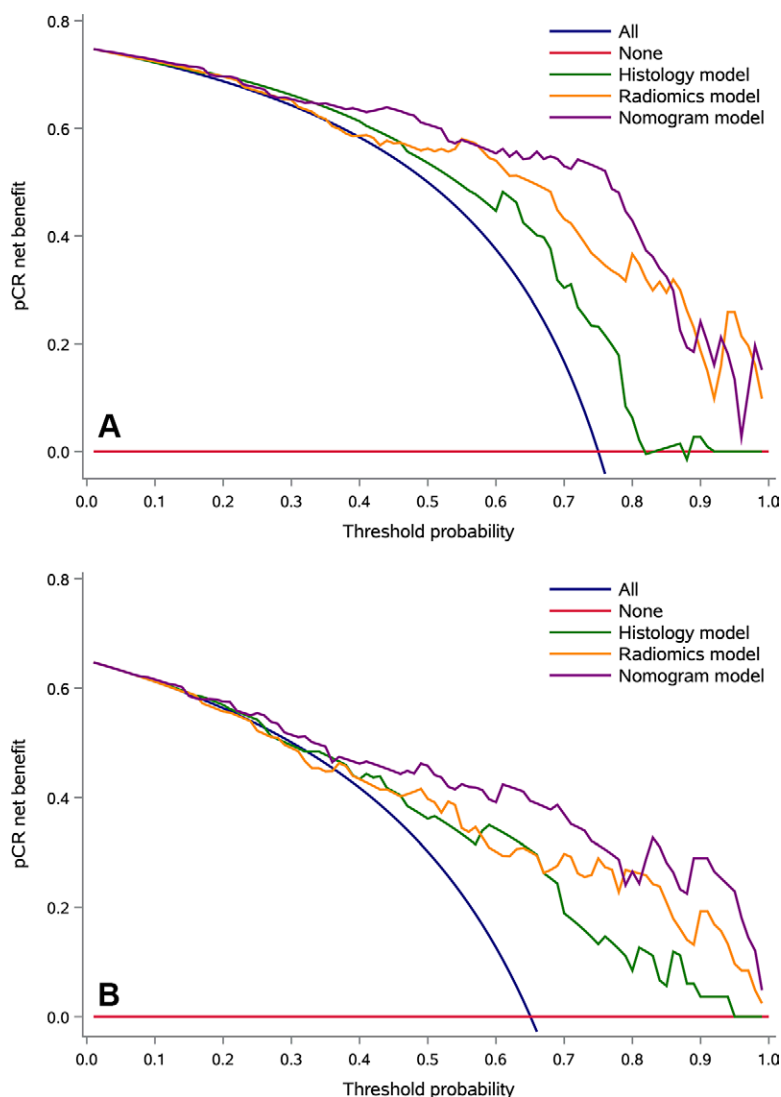


Figure 6: Decision curve analysis for each model in the (A) training set and (B) external test set. The decision curves show that if the threshold probability is over 50%, applying the radiomics or nomogram model to predict pathologic complete response (pCR) adds more benefit than treating all or none of the participants or applying the histologic model to predict pCR.

promising pCR rate of 58% in the single-arm NeopACT trial, and this rate could potentially be improved with radiomics score–guided management (23).

Our radiomics score included sphericity as a shape-based characteristic indicating tumor roundness. This validates a previous study suggesting an increased likelihood of achieving pCR in patients with cancer with smoother margins (24). The importance of appraising intratumoral spatial heterogeneity was highlighted by discriminative features derived from run length and size zone matrices. Inhomogeneity in microvascular perfusion and permeability, as indicated by gray level nonuniformity and first order maximum value on the K^{trans} map, was associated with a lower probability of pCR. Conversely, finer texture—suggested by small area emphasis and short run high gray level emphasis on the Slope_{max} map and size zone nonuniformity on the K^{trans} map—was associated with a greater rate of pCR. These results align with recent findings indicating that tumoral heterogeneity in multicellular

spatial organization can predict anti-programmed death 1 therapy efficacy in TNBC (25).

Prior studies of radiomics at pretreatment dynamic contrast-enhanced MRI in patients with breast cancer undergoing NAC demonstrated the potential to predict pCR, with AUCs ranging from 0.71 to 0.87 (14,15,26–29). However, these studies often relied on retrospective cohorts, typically with small sample sizes within each molecular subtype—especially for TNBC (19%–29% of all patients)—and low pCR rates (21%–40% for the TNBC subtype) that do not align with current realities. Additionally, two recent studies have highlighted the potential predictive value of combining radiomics with genomics or pathologic features in moderate-sized TNBC cohorts treated with NAC, although these findings still require external validation for confirmation (30,31). Further investigation into the agnostic role of radiomics scores in early-stage TNBC is warranted, not only in patients treated with conventional NAC but also in patients treated with the newly established standard NACI.

To assess the biologic basis of the radiomics score, we explored its association with markers of tumor immunogenicity and routine imaging descriptors. There was a relationship between a higher radiomics score and programmed death ligand 1 combined positive score. This finding is consistent with whole-exome sequencing studies showing that highly heterogeneous tumors are associated with decreased activation of the immune response and worse survival in patients with breast cancer (32). Moreover, the radiomics score was negatively associated with androgen receptor–enriched cancer, suggesting that this subtype may have partial chemoimmunoresponse (33).

Some limitations of this study should be noted. First, the MRI scans used had high spatial resolution but limited temporal resolution—as low as 1 minute—requiring the use of the simplest pharmacokinetic model and the extraction of the measured arterial input function. Despite this, studies have indicated that kinetic parameter analysis with limited temporal resolution (exceeding 20 seconds) using the Tofts model remains valuable (19,34). Second, we were not able to assess event-free survival according to the radiomics score because of insufficient follow-up data, leaving a gap in our understanding of long-term outcomes. Third, our radiomics score may have predictive value for the KEYNOTE-522 regimen, but as newer immunotherapies emerge, its use will require further testing in other cohorts. Finally, incorporating multimodal functional imaging, such as PET/CT, might further improve radiomics score performance (35).

A radiomics score at pretreatment perfusion MRI effectively predicted pathologic complete response in patients with triple-negative breast cancer treated with immunotherapy-based regimens, showing potential to serve as a biomarker for heterogeneity in drug sensitivity for future de-escalation studies.

Deputy Editor: Linda Moy

Scientific Editor: Elizabeth Weintraub

Author contributions: Guarantors of integrity of entire study, **T.R., V.L., E.L., A.V.S., H.J.B., A.T.**; study concepts/study design or data acquisition or data analysis/interpretation, all authors; manuscript drafting or manuscript revision for important intellectual content, all authors; approval of final version of submitted manuscript, all authors; agree to ensure any questions related to the work are appropriately resolved, all authors; literature research, **T.R., V.L., C.B., M.J., E.M., D.B.R., F.M.G., A.V.S., L.C., A.T.**; clinical studies, **V.L., C.B., E.M., D.B.R., F.C.B., A.L., C.M.**; experimental studies, **C.B., M.J., E.M., D.B.R.**; statistical analysis, **T.R., C.B., E.M., E.L., D.B.R.**; and manuscript editing, **T.R., V.L., C.B., E.M., J.S., E.L., E.R., D.B.R., A.V.S., F.C.B., A.L., C.M., L.C., H.J.B., A.T.**

Disclosures of conflicts of interest: **T.R.** No relevant relationships. **V.L.** No relevant relationships. **C.B.** No relevant relationships. **M.J.** No relevant relationships. **E.M.** No relevant relationships. **J.S.** No relevant relationships. **E.L.** No relevant relationships. **E.R.** Grants or contracts from Bristol Myers Squibb, AstraZeneca, Replimune, and Janssen; consulting fees from Roche; and support for attending meetings and/or travel from MSD and Roche. **D.B.R.** No relevant relationships. **F.M.G.** No relevant relationships. **A.V.S.** Grants or contracts from Ibex Medical Analytics, AstraZeneca, Primaa, MSD Avenir, and Owkin; consulting fees from Ibex Medical Analytics; payment or honoraria for lectures, presentations, speakers bureaus, manuscript writing, or educational events from Ibex Medical Analytics, AstraZeneca, Primaa, MSD, Roche, Novartis, Leica, Agena, Exact Sciences, NanoString, Daiichi Sankyo, and Myriad Genetics; support for attending meetings and/or travel from Ibex Medical Analytics; and stock or stock options from Ibex Medical Analytics. **F.C.B.** Grants or contracts from AstraZeneca and MSD; consulting fees from AstraZeneca and Gilead; payment or honoraria for lectures, presentations, speakers bureaus, manuscript writing, or educational events from AstraZeneca; and support for attending meetings and/or travel from AstraZeneca. **A.L.** No relevant relationships. **C.M.** No relevant relationships. **L.C.** No relevant relationships. **H.J.B.** No relevant relationships. **A.T.** No relevant relationships.

References

- Garrido-Castro AC, Lin NU, Polyak K. Insights into molecular classifications of triple-negative breast cancer: improving patient selection for treatment. *Cancer Discov* 2019;9(2):176–198.
- Cardoso F, Kyriakides S, Ohno S, et al. Early breast cancer: ESMO clinical practice guidelines for diagnosis, treatment and follow-up. *Ann Oncol* 2019;30(8):1194–1220. [Published corrections appear in *Ann Oncol* 2019;30(10):1674 and *Ann Oncol* 2021;32(2):284.]
- Korde LA, Somerfield MR, Carey LA, et al. Neoadjuvant chemotherapy, endocrine therapy, and targeted therapy for breast cancer: ASCO guideline. *J Clin Oncol* 2021;39(13):1485–1505.
- Yau C, Osdoit M, van der Noordaa M, et al. Residual cancer burden after neoadjuvant chemotherapy and long-term survival outcomes in breast cancer: a multicentre pooled analysis of 5161 patients. *Lancet Oncol* 2022;23(1):149–160.
- Schmid P, Cortes J, Pusztai L, et al. Pembrolizumab for early triple-negative breast cancer. *N Engl J Med* 2020;382(9):810–821.
- Schmid P, Cortes J, Dent R, et al. Event-free survival with pembrolizumab in early triple-negative breast cancer. *N Engl J Med* 2022;386(6):556–567.
- Gonzalez-Ericsson PI, Stovgaard ES, Sua LF, et al. The path to a better biomarker: application of a risk management framework for the implementation of PD-L1 and TILs as immuno-oncology biomarkers in breast cancer clinical trials and daily practice. *J Pathol* 2020;250(5):667–684.
- Rugo HS, Loi S, Adams S, et al. PD-L1 immunohistochemistry assay comparison in atezolizumab plus nab-paclitaxel-treated advanced triple-negative breast cancer. *J Natl Cancer Inst* 2021;113(12):1733–1743.
- Karn T, Denkert C, Weber KE, et al. Tumor mutational burden and immune infiltration as independent predictors of response to neoadjuvant immune checkpoint inhibition in early TNBC in GeparNuevo. *Ann Oncol* 2020;31(9):1216–1222.
- Burstein MD, Tsimelzon A, Poage GM, et al. Comprehensive genomic analysis identifies novel subtypes and targets of triple-negative breast cancer. *Clin Cancer Res* 2015;21(7):1688–1698.
- Jiang YZ, Ma D, Suo C, et al. Genomic and transcriptomic landscape of triple-negative breast cancers: subtypes and treatment strategies. *Cancer Cell* 2019;35(3):428–440.e5.
- Dagogo-Jack I, Shaw AT. Tumour heterogeneity and resistance to cancer therapies. *Nat Rev Clin Oncol* 2018;15(2):81–94.
- Wu J, Gong G, Cui Y, Li R. Intratumor partitioning and texture analysis of dynamic contrast-enhanced (DCE)-MRI identifies relevant tumor subregions to predict pathological response of breast cancer to neoadjuvant chemotherapy. *J Magn Reson Imaging* 2016;44(5):1107–1115.
- Wu J, Cao G, Sun X, et al. Intratumoral spatial heterogeneity at perfusion MR imaging predicts recurrence-free survival in locally advanced breast cancer treated with neoadjuvant chemotherapy. *Radiology* 2018;288(1):26–35.
- Shi Z, Huang X, Cheng Z, et al. MRI-based quantification of intratumoral heterogeneity for predicting treatment response to neoadjuvant chemotherapy in breast cancer. *Radiology* 2023;308(1):e222830.
- Bossuyt PM, Reitsma JB, Bruns DE, et al. STARD 2015: an updated list of essential items for reporting diagnostic accuracy studies. *Radiology* 2015;277(3):826–832.
- Li W, Newitt DC, Gibbs J, et al. Predicting breast cancer response to neoadjuvant treatment using multi-feature MRI: results from the I-SPY 2 TRIAL. *NPJ Breast Cancer* 2020;6(1):63.
- D'Orsi CJ, Sickles EA, Mendelson EB, et al. ACR BI-RADS atlas: Breast Imaging Reporting and Data System. 5th ed. Reston, Va: American College of Radiology, 2013.
- de Bazelaire C, Calmon R, Thomassin I, et al. Accuracy of perfusion MRI with high spatial but low temporal resolution to assess invasive breast cancer response to neoadjuvant chemotherapy: a retrospective study. *BMC Cancer* 2011;11(1):361.
- Documentation/4.5/Modules/PkModeling. Slicer Wiki. <https://www.slicer.org/wiki/Documentation/4.5/Modules/PkModeling>. Updated November 12, 2015. Accessed January 30, 2022.
- van Griethuysen JJM, Fedorov A, Parmar C, et al. Computational radiomics system to decode the radiographic phenotype. *Cancer Res* 2017;77(21):e104–e107.
- Li JY, Chen YP, Li YQ, Liu N, Ma J. Chemotherapeutic and targeted agents can modulate the tumor microenvironment and increase the efficacy of immune checkpoint blockades. *Mol Cancer* 2021;20(1):27.
- Sharma P, Stecklein SR, Yoder R, et al. Clinical and biomarker findings of neoadjuvant pembrolizumab and carboplatin plus docetaxel in triple-negative breast cancer: NeOPACT phase 2 clinical trial. *JAMA Oncol* 2024;10(2):227.
- Li W, Newitt DC, Yun B, et al. Tumor sphericity predicts response in neoadjuvant chemotherapy for invasive breast cancer. *Tomography* 2020;6(2):216–222.
- Wang XQ, Danenberg E, Huang CS, et al. Spatial predictors of immunotherapy response in triple-negative breast cancer. *Nature* 2023;621(7980):868–876.
- Choudhery S, Gomez-Cardona D, Favazza CP, et al. MRI radiomics for assessment of molecular subtype, pathological complete Response, and residual cancer burden in breast cancer patients treated with neoadjuvant chemotherapy. *Acad Radiol* 2022;29(Suppl 1):S145–S154.
- Cain EH, Saha A, Harowicz MR, Marks JR, Marcom PK, Mazurowski MA. Multivariate machine learning models for prediction of pathologic response to neoadjuvant therapy in breast cancer using MRI features: a study using an independent validation set. *Breast Cancer Res Treat* 2019;173(2):455–463.
- Liu Z, Li Z, Qu J, et al. Radiomics of multiparametric MRI for pretreatment prediction of pathologic complete response to neoadjuvant chemotherapy in breast cancer: a multicenter study. *Clin Cancer Res* 2019;25(12):3538–3547.
- Caballo M, Sanderink WBG, Han L, Gao Y, Athanasios A, Mann RM. Four-dimensional machine learning radiomics for the pretreatment assessment of breast cancer pathologic complete response to neoadjuvant chemotherapy in dynamic contrast-enhanced MRI. *J Magn Reson Imaging* 2023;57(1):97–110.
- Jimenez JE, Abdelhazef A, Mittendorf EA, et al. A model combining pretreatment MRI radiomic features and tumor-infiltrating lymphocytes to predict response to neoadjuvant systemic therapy in triple-negative breast cancer. *Eur J Radiol* 2022;149:110220.
- Zhang Y, You C, Pei Y, et al. Integration of radiogenomic features for early prediction of pathological complete response in patients with triple-negative breast cancer and identification of potential therapeutic targets. *J Transl Med* 2022;20(1):256.
- McDonald KA, Kawaguchi T, Qi Q, et al. Tumor heterogeneity correlates with less immune response and worse survival in breast cancer patients. *Ann Surg Oncol* 2019;26(7):2191–2199.
- Mohammed AA, Elsayed FM, Algazar M, Rashed HE, Anter AH. Neoadjuvant chemotherapy in triple negative breast cancer: correlation between androgen receptor expression and pathological response. *Asian Pac J Cancer Prev* 2020;21(2):563–568.
- Planey CR, Welch EB, Xu L, et al. Temporal sampling requirements for reference region modeling of DCE-MRI data in human breast cancer. *J Magn Reson Imaging* 2009;30(1):121–134.
- Seban RD, Arnaud E, Loirat D, et al. [18F]FDG PET/CT for predicting triple-negative breast cancer outcomes after neoadjuvant chemotherapy with or without pembrolizumab. *Eur J Nucl Med Mol Imaging* 2023;50(13):4024–4035.